Remote Sensing of Environment 204 (2018) 872–882

Contents lists available at ScienceDirect

Remote Sensing of Environment

journal homepage: www.elsevier.com/locate/rse

Improving Lidar-based aboveground biomass estimation of temperate hardwood forests with varying site productivity

Gang Shao[a,*], Guofan Shao[a], Joey Gallion[b], Michael R. Saunders[a], Jane R. Frankenberger[c], Songlin Fei[a]

[a] Department of Forestry and Natural Resources, Purdue University, 195 Marsteller Street, West Lafayette, IN 47907, USA
[b] Indiana Department of Natural Resources, 1278 E State Road 250, Brownstown, IN 47220, USA
[c] Department of Agricultural and Biological Engineering, Purdue University, 225 S State Street, West Lafayette, IN 47907, USA

ARTICLE INFO

Keywords:
Biomass
Lidar
Forest inventory
Site index
AGB
Central hardwood forests
Temperate hardwood forests
Forest productivity
Soil map

ABSTRACT

Accurate quantification of forest aboveground biomass (AGB) is the foundation to the responses of diverse forest ecosystems to the changing climate. Lidar-based statistical models have been used to accurately estimate AGB in large spatial extents, especially in boreal and temperate softwood forest ecosystems. However, the few available models for temperate hardwood and hardwood-dominated mixed forests are low in accuracy due both to the deliquescent growth form of hardwood trees and the strong site-to-site variations in height-diameter relationship. In this study, we established multiplicative nonlinear regression models that incorporated both lidar-derived metrics and soil-based site productivity classes (high and low productivity sites) to estimate aboveground biomass in temperate hardwood forests. The final optimized model had high accuracy (R^2 = 0.81; RMSE = 45.5 Mg ha^{-1}) with reliable performance in ABG estimation by integrating relative height metrics at 75 and 70 percentiles (RH75 and RH70), canopy coverage and site productivity class. An optimized model that included an index of site productivity explained 14% more variance than the best-fit model without the term. Moreover, the relationship between AGB and lidar-based metrics was nonlinear on low productivity sites and nearly linear on high productivity sites, further indicating the importance of including direct or indirect measures of site productivity in lidar-based biomass models, particularly for those applied to temperate hardwood forests. Our new lidar-based model provides a potential framework to integrate lidar-based structural information and soil-based site productivity to improve AGB estimation in temperate hardwood forests.

1. Introduction

Lidar (Light detection and ranging) is considered as a promising technology to quantify and monitor aboveground biomass (AGB) in forest ecosystems, providing essential information to understand their dynamics in response to a set of grand challenges such as climate change, invasive species, and land use change (Lim et al., 2003; Wulder et al., 2012). Previous studies have utilized lidar-based forest structure metrics with statistical modeling to successfully estimate AGB in boreal forests (Huang et al., 2013; Montesano et al., 2014; Næsset et al., 2011; Popescu, 2007), temperate softwood/softwood-dominated mixed forests (Hudak et al., 2012; Pflugmacher et al., 2012; Zhao et al., 2009) and tropical/subtropical hardwood forests (Asner et al., 2010; Cao et al., 2016; Ferraz et al., 2016; Kronseder et al., 2012). However, few studies have presented desirable AGB estimations in temperate hardwood and hardwood-dominated mixed forests.

Existing lidar-based models are often challenged by either relatively low accuracy (i.e., low R^2 values) or unreliable model performance (i.e., high RMSE value) in estimating AGB in temperate hardwood and mixed forests (see Table A1 in Appendix). For example, Anderson et al. (2006) applied single linear regression using a relative height metric (RH50) to estimate AGB in temperate mixed forests in New Hampshire, USA with a R^2 of 0.41. Lim and Treitz (2004) employed the power function and RH metrics to predict AGB distribution in temperate mixed forests in Ontario, Canada, which has a relatively high accuracy (R^2 = 0.90) but with low reliability (RMSE = 50.2 Mg ha^{-1}). Duncanson et al. (2015) included individual-tree metrics in multiple linear models to estimate AGB estimation in three temperate forests across USA but required high density returns (50 pts. m^{-2} in this study). Though the availability of high return density lidar campaigns is increasing worldwide to address ecological and environmental questions, these data are still associated with intensive computation and limited spatial coverage (Duncanson et al., 2014; Popescu et al., 2003).

The challenges for accurate modeling of AGB in temperate

* Corresponding author.
E-mail address: shaogang@msu.edu (G. Shao).

http://dx.doi.org/10.1016/j.rse.2017.09.011
Received 23 November 2016; Received in revised form 8 August 2017; Accepted 13 September 2017
Available online 09 October 2017

hardwood forests are multifold. First, lidar-based AGB estimations typically rely on height metrics as primary model predictors/variables (Zolkos et al., 2013). The deliquescent growth form of hardwood trees challenges height-based metrics due to the similarity of the vertical height profiles with varied tree volume/density (Banskota et al., 2011; Boudreau et al., 2008). Second, the varied site productivity disperses height-diameter relationships in different forest sites (Skovsgaard and Vanclay, 2008) and across different species, which make it difficult to derive height-based lidar metrics to estimate diameter-based field-observed AGB (Jenkins et al., 2003). Site productivity has traditionally been derived from the height growth of overstory trees, as tree height growth have been viewed to better integrate the effects of climate, soil, terrain and other edaphic conditions (Skovsgaard and Vanclay, 2013) than diameter growth. Therefore, site productivity, either direction or through inclusion of tree height as a covariate modifying the power relationship between AGB and diameter, has been included in many allometric equation based AGB studies (e.g. site productivity is related to the power parameter b in the form $A = aD^b$, where A and D stand for AGB and diameter respectively, a and b are model parameters) (Basuki et al., 2009; Chave et al., 2014; Ketterings et al., 2001). However, differences in the height-diameter relationship with site are barely considered in most lidar-based AGB estimations. Therefore, it is necessary to establish a reliable lidar-based model regarding both the canopy structure and site productivity to reduce the uncertainties in AGB estimations.

Here, we develop a reliable and robust lidar-based regression model to predict AGB in mixed hardwood forests in the Central Hardwood Forest region in eastern USA. Specifically, we aim to (1) determine robust lidar metrics for AGB estimation; (2) investigate the impacts of site variances on AGB estimation by incorporating site productivity classes (high and low productivity sites) in lidar-based models; and (3) test the accuracy and reliability of the optimized model. Our study provides a valuable framework on which others may optimize the lidar-based AGB estimation models in temperate hardwood forests with regards to site productivity effects.

2. Material and methods

2.1. Study area

The study was located in the Yellowwood State Forest (YSF), in southern Indiana, USA (39.2° N, 86.3° W) (Fig. 1). The YSF falls into the humid continental climate region with warm-wet summers (21 to 27 °C) and cold winters (−4 to 2 °C). The topography of this unglaciated region is complex, abounding with hills and knolls; elevation ranges from 167 to 300 m with mean slope of 39.1%. The study area is dominated by temperate hardwood forests with a small portion of conifer (mostly pine, *Pinus* spp.) plantations. Dominant species include northern red oak (*Quercus rubra*), white oak (*Q. alba*), black oak (*Q. veluntina*), shagbark hickory (*Carya ovata*), tulip-poplar (*Liriodendron tulipifera*), and sugar maple (*Acer saccharum*). Multiple silvicultural treatments in these sites have created a diverse array of forest canopy structures, varying greatly in both horizontal and vertical dimensions.

2.2. Field plot data

Forest inventory data were collected in Compartment 2 of the YSF between January and March in 2010 (Gallion, 2012) (Fig. 1) as part of the Indiana Department of Natural Resources – Division of Forestry continuous forest inventory (CFI) effort. The CFI sampling methodology largely followed the procedures of U.S. Forest Inventory Analysis (FIA) program but with different plot size and sampling intensity. Each FIA plot has four subplot with 7.3 m radius in every 2428 ha (6000 acres), while each CFI plot has one 7.3 m plot radius every16.2 ha (one per every 40 acres) (Shao et al., 2014). All trees with diameter at breast height (DBH) of ≥ 12.7 cm (5 in.) within CFI plot were measured. Further detailed inventory methods are in Gallion (2012). For this study, we extracted measurements of DBH, tree height, and dominated-species-based site productivity from 59 CFI plots within study area. Field-based AGB observations were first estimated at the tree-level using species-specific Jenkins et al. (2003) DBH allometric equations. The AGB of each tree within inventory plots were then summed for plot-level AGB.

2.3. Lidar data and soil map

Airborne lidar data was acquired from the Indiana Statewide Lidar program (2011–2013 Indiana Statewide Lidar, 2016). The data covering the study area was collected in 2011 during the leaf-off season. An Optech Gemini Lidar system (ALS50) was used to collect multiple returns lidar with 99 kHz of pulse repetition rate, 40° of scan angle and 35.8 Hz of scan frequency. The laser system was flown 2000 m above ground, resulted in a 1731 m swath width with 20–30% overlap and an averaged 1.4 pts m^{-2} point density. Both canopy height model (CHM) and digital elevation model (DEM) were generated at 1-m resolution with all returns using FUSION/LDV software system developed by the

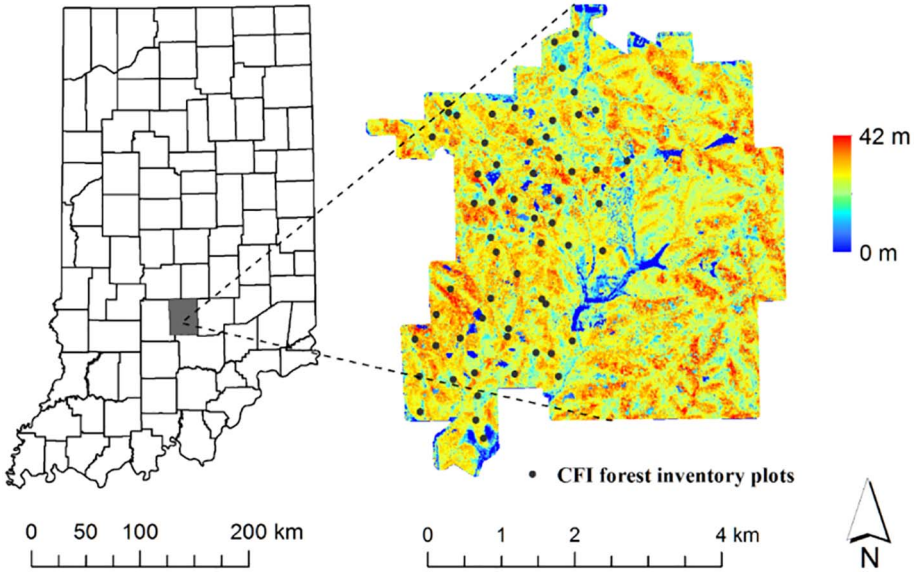

Fig. 1. Canopy height model (CHM) of the study area (on the right), located in the southeast part of Yellowwood State Forest in Indiana, USA (Indiana state map on the right). Black dots stand for the locations of forest inventory plots used in this study.

Table 1
Soil units from gSSURGO dataset, black oak site index from CFI plots and productivity classification in this study.
** Productivity class that was classified using canopy height information from CHM.*

Soil unit symbol	Area (Ha)	Taxonomic class	Slope (%)	Black Oak SI (Age 50)	Productivity class
BgF	1623.9	Loamy-skeletal, mixed, active, mesic Typic Dystrudepts	20–70	77	High
WaD	446.1	Fine-silty, mixed, active, mesic Typic Hapludults	6–20	68	Low
Be	176.9	Loamy-skeletal, mixed, active, mesic Fluventic Dystrudepts	1–3	76	High
TlB	47.8	Fine-silty, mixed, active, mesic Typic Fragiudults	2–6	–	Low*
Hc	9.8	Coarse-silty, mixed, superactive, mesic Dystric Fluventic Eutrudepts	0–2	–	Low*
WeC2	9.4	Fine-silty, mixed, active, mesic Typic Hapludults	6–20	79	High
SxD2	6.4	Fine-silty, Mixed, semiactive, mesic Typic Hapludults	10–20	–	Low*
Sv	2.3	Fine-silty, mixed, active, acid, mesic Fluventic Endoaquepts	0–2	–	Low*
Sf	1.2	Fine-silty, mixed, active, mesic Fluvaquentic Dystrudepts	0–2	–	Low*

U.S. Forest Service (FUSION 3.6, 2016). First, ground points were filtered (Kraus and Pfeifer, 1998) and interpolated (inverse distance weighted interpolation) into DEM. Aboveground heights of lidar points were calculated by subtracting DEM values from elevations to generate CHM. Then, a series of morphological image processing operations, dilation followed by erosion, were applied on CHM to fill the 'holes/data-gaps' in canopy surface (Chen et al., 2006; Zhang et al., 2003).

The Gridded Soil Survey Geographic Database (gSSURGO) 2016 was used as soil map to assist site productivity characterization across the study area. The soil map was downloaded from the geospatial data gateway of Natural Resources Conservation Service (NRCS, 2016). This dataset integrates in-field survey and remote sensing technologies, and is considered the most detailed national-level soil map in the U.S. with a spatial resolution of 10 m. The forested areas in our study site covered nine gSSURGO soil units (Table 1). Among which, five units belong to the soil order of inceptisols and four units belong to the order of Ultisols (Fig. 2).

2.4. Lidar metrics generation and selection

We derived several plot-level lidar metrics as potential variables for our AGB estimation model. Height-based metrics included relative heights metrics (RH), maximum (MaxH), mean (MeanH), minimum height (MinH), and the standard deviation of heights (SDH). Density-based metrics included canopy coverage (CC), first-return-based canopy closure (FR_CC) and canopy relief ratio (CRR) ((MeanH-MinH)/(MaxH-MinH)). Geography-based metrics included elevation (Elev), slope and aspect. Most lidar metrics, except for CC and all geography-based metrics, were derived using the lidar points within each inventory plot through GridMetrics function in FUSION/LDV software (FUSION 3.6, 2016). The CC were calculated based on 1-m canopy height model (CHM), and defined as the coverage of canopy above 10 m (Stark et al., 2012; Vepakomma et al., 2008). Geography-based metrics (e.g. Elev, slope and aspect) were calculated using a digital elevation model (DEM). Because this lidar data was low density, we did not calculate

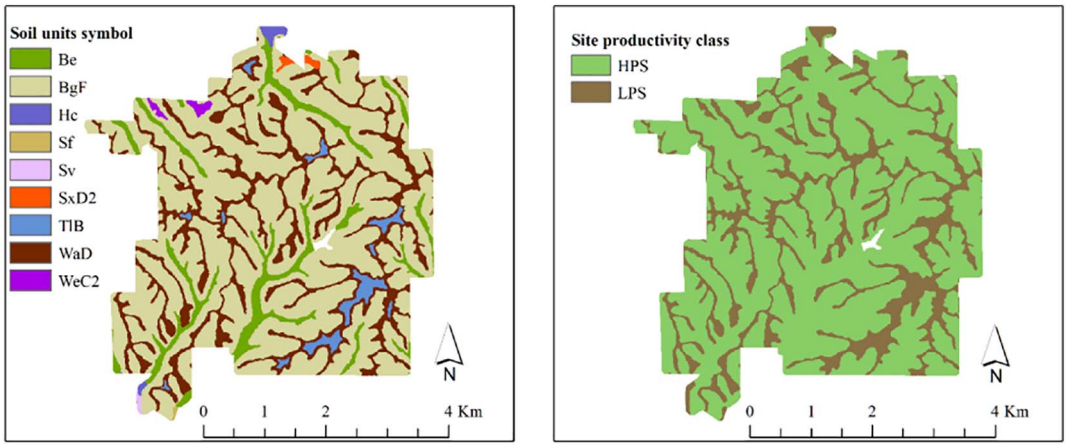

Fig. 2. The soil map of the study area from gSSURGO (left) and the site productivity map derived based on the soil map and forest inventory data (right). Information for soil units can be found in NRCS (2016); HPS – high rpoductivty site, LPS – low productivity site.

any commonly-used metrics that are sensitive to point density and flight line overlaps (e.g. Density deciles, which are the number of lidar points within percentile heights) (Jakubowski et al., 2013) or any individual tree-level metrics (e.g. tree heights or crown size). Additionally, we did not calculate intensity-related metrics (e.g. mean first return intensity) because the lidar was collected during leaf-off season where intensities are mainly reflections of stems and branches of trees.

2.5. Site productivity classification

We classified soil units within the study area into productivity classes using a gSSURGO-based soil map and through calculation of site index (SI) with CFI data. Soil units were used to represent site productivity units at this regional scale by assuming edaphic factors control tree growth under similar local climates. SI value of each soil unit were calculated using the average SI value of CFI plots within each soil unit. As SI is a species-specific index as species vary in height growth patterns as site productivity increases. We only selected the CFI plots with black oak, a very common species within the study area found on 27 of our 59 CFI plots and calculated the SI of soil units. This procedure allowed us to classify four soil units that covered over 97% of the study area and all CFI plots. CFI plots fell into two of the six site productivity classes in the CFI dataset (Class 4 and 5, split at a $SI_{base\ age\ =\ 50}$ threshold of 72 ft) (Table 1). Therefore, we re-classified the soil units into two classes: 1. high productivity sites (HPS) if their SI_{50} was > 72 and 2. low productivity sites (LPS) if their SI_{50} was equal or < 72 (Fig. 2). Soil units without information of forest productivity or CFI plots (< 3% of the study areas) were manually assigned productivity class by comparing their CHM-derived average canopy height of mature forests in those units and assigning the unit to the productivity class with similar mean canopy height (Table 1).

2.6. Basic model establishments and variable selection

In this study, a power relationship was observed in correlating observed AGB with RH metrics and used as the basic function in the regression model (Lim and Treitz, 2004) (Eq. 1).

$$AGB = \beta_0 X_1^{\beta_1} \quad (1)$$

where X_1 is the selected lidar metric, and β_0 and $\beta_1$are parameters to be estimated. To fully exploit the lidar metrics, we used a multiplicative nonlinear regression model following Næsset et al. (2011) (Eq. (2)).

$$AGB = \beta_0 X_1^{\beta_1} X_2^{\beta_2} \ldots X_n^{\beta_n} \quad (2)$$

where X_1, X_2, …, X_n are the lidar-metric variables and β_0, β_1, β_2, …, β_n are parameters to be estimated. The coefficients in this model were estimated using linear regression model in logistic transformation (Næsset et al., 2011).

To select robust variables from all derived lidar metrics, we used the Random Forest (RF) algorithm using randomForest package (Liaw and Wiener, 2002) in the R language (R Development Core Team, v3.3.1). RF is a learning approach to generate numerous decision trees for classification and regression. It utilizes bootstrapping technique to generate random inputs to increase the accuracy of the regression. In this study, RF ranked lidar metrics using regression importance values, which were calculated by the impacts of lidar metrics on estimation accuracy and residuals. Based on the regression importance values, we selected the top ten sensitive metrics (large impacts on estimation accuracy and residuals) as candidates variables for the AGB estimation models (Hudak et al., 2012). The best combination of lidar metrics searched by RF was then used to establish a set of preliminary AGB estimation model. A stepwise regression approach was then employed to search the best fit model using the remaining lidar metrics from the preliminary AGB model.

2.7. Model optimization

To improve the estimation performance, we made two adjustments to the basic regression models to increase the accuracy of estimation or reduce the root mean squared error (RMSE) in estimated AGB.

First, we weighted height metrics using selected canopy coverage-based metrics such as canopy coverage, canopy closure and canopy relief ratio (Eq. (3)).

$$AGB = \beta_0 X_1^{w_1\beta_1} X_2^{w_2\beta_2} \ldots X_n^{w_n\beta_n} \quad (3)$$

where w_n is a weight for each β_n. To avoid overfitting, we arbitrarily restricted the model to no more than one weight parameter in the model. Weights were selected from the ranked RF candidates and added to one variable term at a time. The weight had the potential to change the importance rank of variables, so it was necessary to substitute variables to search the best fit model. In this step, we used interactive stepwise regression approach to iteratively adjust the model with the available variable combinations after previous feature selection. This supervised approach helped find optimized models with ecologically meaningful equations.

The second adjustment was to add a dummy variable (D) related to the HPS (value of 1) and LPS (value of 0) productivity classes derived from CFI and gSSURGO data (Fig. 2). The dummy variable was associated with the power parameters in allometric equations (Chave et al., 2014) as we discussed in introduction. The final model, therefore, was (Eq. (4)):

$$AGB = \beta_0 X_1^{w_1\beta_1} X_2^{w_1\beta_2} \ldots X_{n-1}^{w_1\beta_{n-1}} X_n^{w_1\beta_n D} \quad (4)$$

This fitting procedure was similar to the weighting adjustments, and we searched the best fit model through the interactive stepwise regression approach. We also added the dummy variable to the basic regression models without weighting the parameters for cross validation.

Fit statistics for all models included R^2, adjusted R^2, root mean square error (RMSE) and relative RMSE (%RMSE) of estimated AGB. Additionally, we fit observed AGB and model-estimated AGB in linear regression (Duncanson et al., 2014). The linear slopes, correlation coefficients and RMSE of those regressions were also used to evaluate the AGB estimations.

2.8. Model validation

Our use of site productivity classes in the model was validated using a combination of lidar-based metrics and field-based observations. Since field-based algorithms relied on DBH to estimate AGB and the lidar-based metrics relied on height to estimate AGB, one could assume that differing height-diameter relationships by site would affect model performance. Therefore, we classified both field-observed tree heights and DBH measurements from CFI dataset into HPS and LPS. Then, using logistic least square regression between tree height and DBH in HPS and LPS, respectively, we calculated the 95% confidence intervals (CI) using a *t*-distribution for both regression models. We also applied the linear regressions at log scale for further investigation. Wald statistic and Likelihood ratio statistic were used to evaluate the differences of the elevations and slopes of these two linear models (Warton et al., 2012).

To investigate the effects of site productivity on lidar-based AGB estimation, we performed paired *t*-test to cross validate the differences of AGB estimations using the basic model (without the regard to site productivity) and the adjusted model (with the regard to site productivity). Additionally, with the regard to site productivity class, our model could utilize different functions to estimate AGB in HPS and LPS. We generated two pseudo model curves for HPS and LPS, to investigate their AGB responses to lidar metrics, especially to the height metrics, which are commonly used as major variables in lidar-based AGB estimation models.

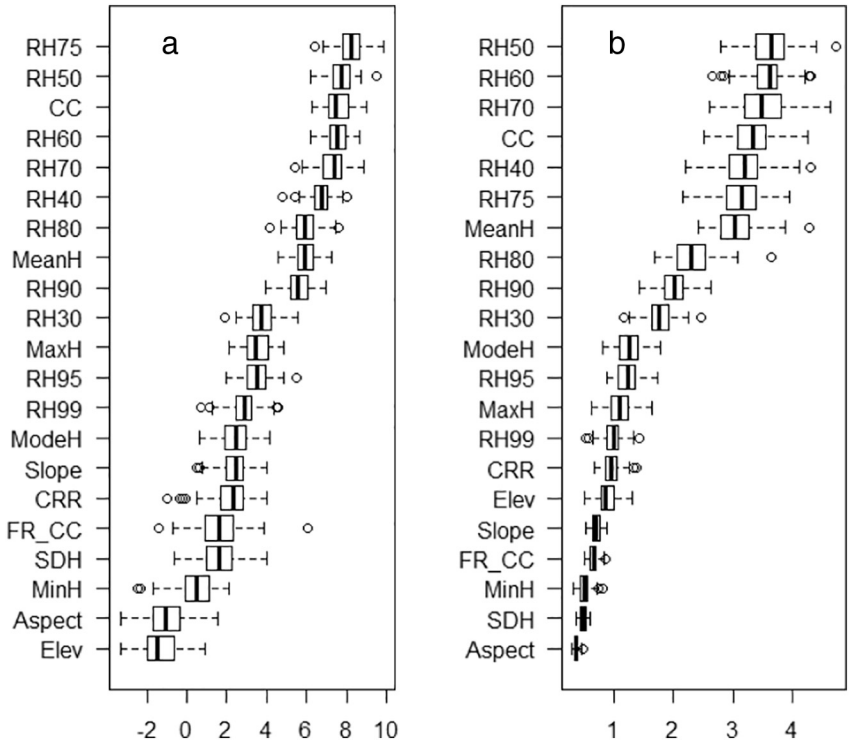

Fig. 3. Radom Forest ranked lidar metrics based on their regression importance values; The R-index (a) is the effects of the variable on estimation accuracy and MSE-index (b) is the effects of the variable on mean squared error. Bold black lines stand for medians, boxes indicate interquartile ranges, whiskers are full ranges and cycles are outliers; Lidar metrics were sorted with their importance values in decreasing order.

To avoid overfitting and explain error of the final established model, we adopted bootstrapping sampling method to simulate the model parameters with random inputs. Random subsets of samples were generated from all 59 plots with six sub-sample sizes (35, 40, 45, 50, 55 and 58). Each sub-sample size was repeated 1000 times and used to estimate the parameters of variables, R^2 and adjusted R^2 of regression model and RMSE of estimated AGB, which were all reported using median values and means with a 95% CI. We also tested the responses of the parameters to the changing sample size in the bootstrapping validation.

3. Results

3.1. AGB estimation from established regression models

Lidar metrics were ranked based on two importance indices from RF: the mean effects in accuracy (R-index) (Fig. 3a) and the mean effects in mean squared error (MSE-index) (Fig. 3b). R-index ranked RH75 as the most important metric with RH 50 as the runner up. MSE-index ranked RH50 the first, followed by RH60 and RH70. CC was the only canopy coverage metric selected by RF, and thus, the only potential weight variable in our model.

Among the basic nonlinear models, multiplicative nonlinear regression produced the best estimation with the combination of RH60 and CC (Basic-M, Table 2). This model had R^2 (Adjusted R^2) value of 0.67 (0.65). RMSE (%RMSE) of estimated AGB was 52.4 Mg ha^{-1} (36%) (Table 2). The linear regression between estimated and observed AGB has a slope of 0.59, R^2 of 0.61 and RMSE of 39.8 Mg ha^{-1} (27%) (Fig. 4).

Among the adjusted models, the final selected regression model contained four variables including a parameter weight (CC) and the site productivity class dummy variable and nine parameters (Adjusted-A and B, Table 2). The major variables were RH75 and RH70, whose parameters were both weighted by CC. The productivity-based dummy variable was added to the RH70 and the constant parameters. This final model had R^2 value of 0.81 (0.78) and RMSE of 45.5 Mg ha^{-1} (31%) (Table 2). The linear regression between estimated and observed AGB has a slope of 0.68, R^2 value of 0.70 and RMSE of 36.8 Mg ha^{-1} (25%) (Fig. 4). This model clearly outperformed the Basic-M model.

3.2. Model validation

There were significant different height-diameter relationships between HPS and LPS, as the 95% CI of these two logistic models did not overlap for trees with DBH > 20 cm (Fig. 5). Wald statistic and Likelihood ratio statistic showed significant differences in elevation ($P < 0.0001$) and insignificant differences in slope ($P = 0.5080$) between these two linear models for HPS and LPS (Fig. A2).

The final adjusted model (Adjusted-A and B) and the best basic model (Basic-M) were selected for paired *t*-test to cross validate the differences of AGB estimations with or without the regard to site productivity in estimation models (Table 3). The paired t-tests showed the differences between these two estimations were significant in LPS ($P = 0.0387$) and insignificant in HPS ($P = 0.2017$) or using all plots ($P = 0.5317$). Comparing Adjusted-A and B model estimated AGB to the observed measurements indicated insignificant differences in both HPS and LPS. Basic-M estimated AGB was insignificantly different from the observed measurements for HPS, but marginally significant for LPS ($P = 0.078$). Additionally, based on the histograms of observed and estimated AGB, the distribution of adjusted model estimated AGB was more close to the distribution of observed measurements, comparing to basic model based estimations (Fig. 6).

Pseudo model curves indicated that different functions for HPS and LPS sites were required to estimate AGB relative to RH70 metrics (Fig. 7). Curves were created using constant CC and fixed ratio between RH75 and RH70 (Eq. (5b)); these showed LPS had a power relationship with the AGB-RH ratio while HPS had a nearly linear relationship. Similar trends were observed in pseudo model curves when using RH70 and CC metrics for AGB estimation and setting ratio between RH75 and RH70 (Eq. (5b)) as constant (Fig. A1).

The bootstrapping validation implied the model had a relatively constant median and explained a large amount of the variation. The median values were always higher than the corresponded means (Fig. 8). As the R^2 and adjusted R^2 were calculated based on the selected

Table 2
Summary of basic and adjusted regression models and AGB estimation.

[$] *Basic-S = basic nonlinear regression using single variable; Basic-M = basic multiplicative nonlinear regression; Adjusted- A = nonlinear regression with weighted parameters; Adjusted-B = nonlinear regression with dummy variable; Adjusted-A and B = nonlinear regression with both weighted parameters and dummy variable.*

[#] *eSlope, eR2, eRMSE and %eRMSE = the slope, correlation coefficient, RMSE and %RMSE of linear regression between estimated and observed AGB, respectively.*

Regression model[$]	Model R2 (Adjusted R^2)	RMSE (Mg ha^{-1})	%RMSE	eSlope[#]	$eR^{2\#}$	eRMSE[#] (Mg ha^{-1})	%eRMSE[#]
Basic-S: $AGB = 0.12*RH50^{2.29}$	0.61 (0.60)	56.4	39%	0.57	0.55	43.3	30%
Basic-M: $AGB = 0.28*RH60^{1.53}*CC^{1.65}$	0.67 (0.65)	52.4	36%	0.59	0.61	39.8	27%
Adjusted-A: $AGB = 0.46*RH75^{(1.22\ +\ 0.65CC)}$	0.66 (0.65)	51.8	36%	0.64	0.61	42.5	29%
Adjusted-B: $AGB = e^{(-3.79\ +\ D)}*CC^{1.42}*RH50^{(2.46-1.62D)}$	0.73 (0.71)	53.7	37%	0.54	0.59	37.6	26%
Adjusted-A and B: $AGB = e^{(0.06\ +\ (8.53-12.64*CC)\ *D)}*RH75^{(-34.12\ +\ 50.22*CC)}*RH70^{(35.11-49.59CC+(-2.16\ +\ 3.24*CC)\ *D)}$	0.81 (0.78)	45.5	31%	0.68	0.70	36.8	25%

samples, they slightly decreased with the increasing sample size. RMSE was calculated using all 59 plots regardless the sample size. The mean RMSE had a significant drop with a far smaller 95% confidence interval when the simulated samples increased from 35 to 40 plots. The varied mean RMSEs and their 95% confidence intervals indicated the model was more reliable when calibrated with > 40 samples. The median RMSE was more stable and always less than mean RMSE (Fig. 8). We also tested the responses of the parameters (labeled as βs in Eqs. 5a and 5b) to the changing sample size in the bootstrapping validation.

$$AGB = e^{(\beta_1+(\beta_2+\beta_3*CC)*D)}*RH75^{(\beta_4+\beta_7*CC)}*RH70^{(\beta_5+\beta_8*CC+(\beta_6+\beta_9*CC)*D)} \quad (5a)$$

$$AGB = e^{(\beta_1+(\beta_2+\beta_3*CC)*D)}*\left(\frac{RH70}{RH75}\right)^{(-\beta_4-\beta_7*CC)} *RH70^{(\beta_5+\beta_4+(\beta_8+\beta_7)*CC+(\beta_6+\beta_9*CC)*D)} \quad (5b)$$

In general, the simulated parameters were relatively stable using different sample sizes (Fig. 9). Uncertainty of all parameters decreased with the increasing sample size, particularly from 40 to 45 plots based on the mean estimations. Similar to the accuracy validation, median values of all parameters were more stable than the means. Among the parameters, the CC weighted parameters (β_3, β_7, β_8, and β_9) had more uncertainty compared to other parameters based on the mean values and 95% confidence intervals. In particular, β_7 and β_8 hold the most

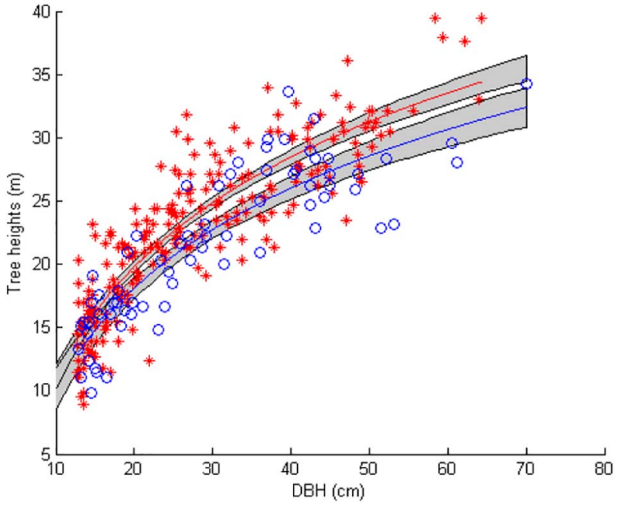

Fig. 5. Logistical least square regression between DBH (x) and tree heights (y) in HPS (red asterisks) and LPS (blue cycles). Solid lines were fitting models; Gray areas were 95% confidence intervals of fitting models. (For interpretation of the references to colour in this figure legend, the reader is referred to the web version of this article.)

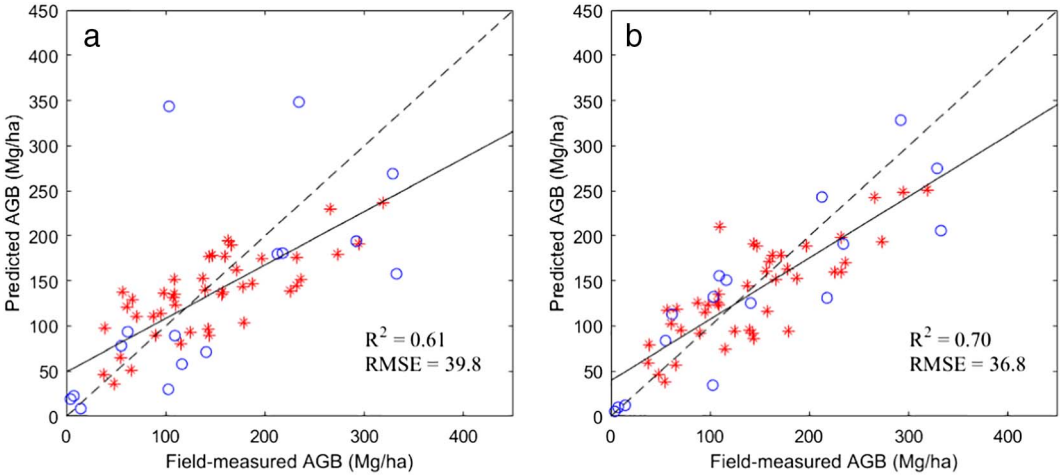

Fig. 4. Linear regressions between observed and estimated AGB using the best basic model (Basic-M) (a) and the best adjusted model (Adjusted-A and B) (b); Red asterisks stand for HPS plots, blue cycles stand for LPS plots, solid line is regression trend line and dash line is y = x. (For interpretation of the references to colour in this figure legend, the reader is referred to the web version of this article.)

Table 3
Paired *t*-tests between AGB estimations using basic and adjusted models and between observed AGB and estimated AGB using both basic and adjusted models.

** HPS = High productivity sites; LPS = Low productivity sites; Basic = Estimated AGB using basic model (Basic-M); Adjusted = Estimated AGB using adjusted model (Adjusted-A and B); Obs. = Observed AGB.*

Plots*	Basic vs adjusted	Obs. vs adjusted	Obs. vs basic
All	0.5317	0.2281	0.1596
HPS	0.2017	0.3089	0.7581
LPS	0.0387	0.5341	0.0783

uncertainty based on the absolute values, yet β_9 was the most uncertain parameter based on the percentage of the variance. Moreover, $\beta_1$was the only parameter with both positive and negative mean values, though its variance was the smallest among all parameters.

4. Discussion

Our study demonstrated that the inclusion of site productivity can greatly improve AGB estimations. Without the inclusion of site productivity, our best basic model (Basic-M) resulted similar AGB estimation accuracy (R^2 = 0.67) to some previous studies with multivariable approaches (R^2 ranging from 0.33 to 0.71) (Banskota et al., 2011; Hawbaker et al., 2009). Including site productivity in the estimation model, the estimation accuracy (R^2 = 0.81; Adjusted R^2 = 0.78) of our final adjusted model (Adjusted-A and B) was higher than most previous studies utilizing similar plot-level metrics (Table A1) and some developed by individual-tree metrics (Duncanson et al., 2015). We estimated that site productivity account for 14% of the unexplained variation in basic model, indicating that site productivity is a robust indicator and provides critical information to improve AGB estimation in lidar-based models.

Compared to basic models, the 5% reduction of RMSE in the optimized model (from 36% to 31%) was not as significant as the improvement of the accuracy. Though the RMSE of 45.5 Mg ha^{-1} (31%) was in the range of previous studies (from 16.3 to 58 Mg ha^{-1} and from 10% to 40%) (Table A1), it was > 20% of observed measurements recommended by Zolkos et al. (2013). There were several reasons for high RMSE in our regression models. First, the plot size of observed data was quite small for AGB estimation (Zolkos et al., 2013), only 0.017 ha. These small plots will have a higher proportion of individuals where lidar-based metric and ground-based sampling does not match, either because individuals with stems inside plots have crowns located partially or fully outside plot boundaries or vice versa (Frazer et al., 2011). Moreover, small plot size was sensitive to co-registration error between observed AGB and lidar metrics. Although we used differential GPS and lidar-based canopy height model updated coordinates of some plots (20 of 59) within heterogeneous canopy surface, the co-registration error between lidar metrics and CFI plots may still affect the AGB estimation. Future study may be required to improve the co-registration of small-size plots by using Bayesian approaches and other advanced learning algorithms.

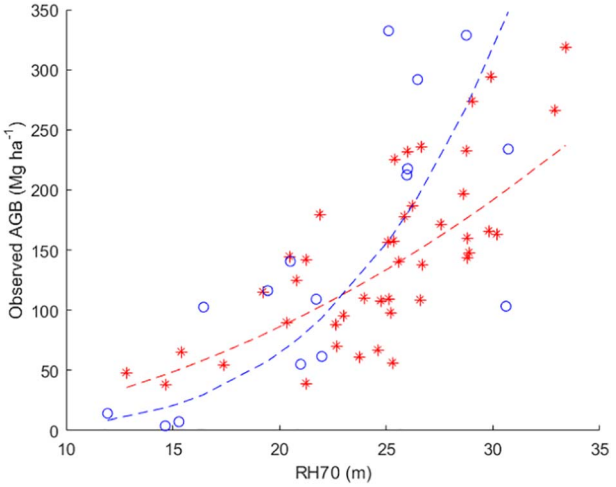

Fig. 7. Pseudo model curves between observed AGB and RH70 (AGB-RH ratio) in HPS (red dash line) and LPS (blue dash line); Red asterisks stand for HPS plots and blue cycles stand for LPS plots. (For interpretation of the references to colour in this figure legend, the reader is referred to the web version of this article.)

Additionally, we feel that our sample size of CFI plots may have been insufficient to capture the variability in AGB found across the study area. Plots with very low and very high AGB were not estimated well (Fig. 4); this may have been caused by the predominantly partial harvesting (i.e., small patch cuttings and selection cuttings) since 2008. This resulted in a number of plots with similar heights profiles but vastly different AGBs. The small sample size made CC insufficient to fully explain the variance in horizontal canopy condition.

Our regression analysis between tree heights and DBH at individual tree level proved significant different height-diameter relationships in HPS and LPS, indicating the AGB have different responses to height metrics in these two condition sites. AGB and RH70 had a power relationship in LPS, yet a nearly linear relationship in HPS, indicating AGB increased faster with height in LPS comparing to HPS. One possible reason of this difference is that trees in LPS may grow slower in height due to resource limitation resulting smaller height-diameter rate compared to HPS. The nearly linear curve in HPS had agreed with some previous studies, which used multiple linear regressions for AGB estimations (Anderson et al., 2006; Banskota et al., 2011; van Aardt et al., 2006). Some of these studies reported similar accuracy as our basic

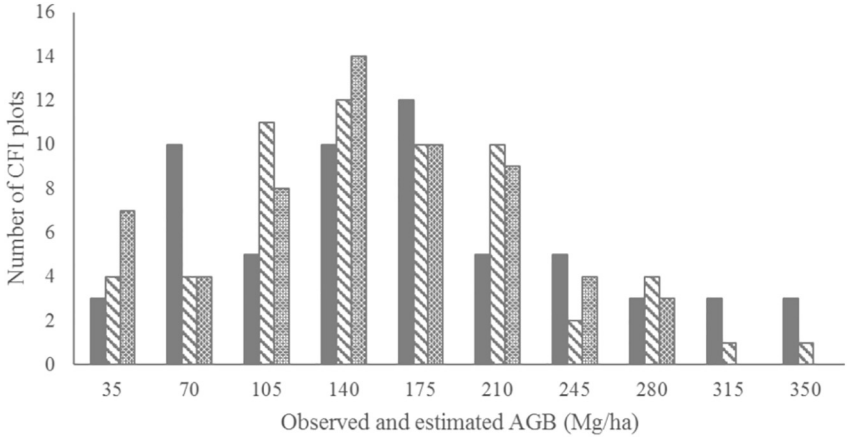

Fig. 6. The distribution of observed AGB (solid-gray bar) and estimated AGB using both selected basic (Basic-M, dotted bar) and adjusted (Adjusted-A and B, diagonal-strip bar) models. In general, the distribution of adjusted model estimated AGB was more close to the distribution of observed measurements, compared to basic model estimated AGB. However, we applied pairwise Kolmogorov-Smirnov test (K-S test) and found differences among these three distributions were statistical insignificant.

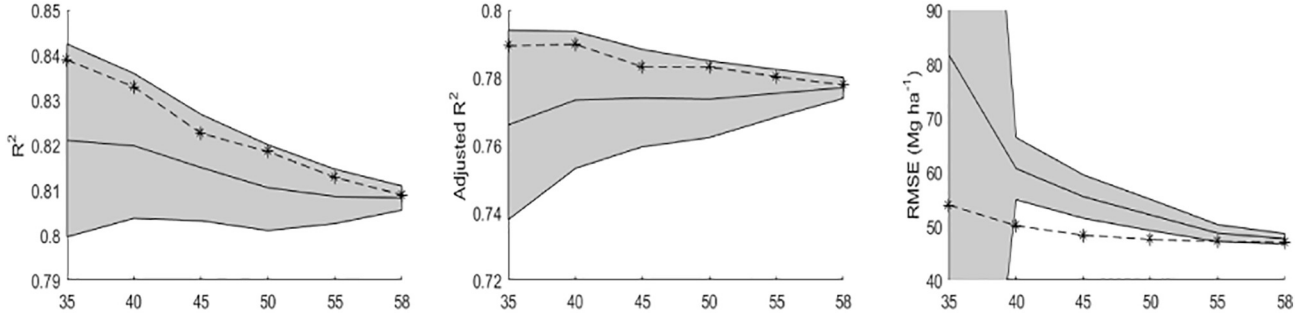

Fig. 8. Median values (dash line) and means with 95% confidence interval (gray area) of R-square, adjusted r-square and RMSE in bootstrapping model validation. Horizontal axis is the number of samples used in model validation. Vertical axis is the resulted values of R-square, adjusted R-square, and RMSE.

model (Basic-M), indicating that the power relationship in LPS might have considerable impacts on the estimation accuracy of linear regression models. Based on our paired *t*-test between observed and estimated AGB values (Table 3), our final adjusted model significantly improved AGB estimations in LPS and therefore improved the overall estimation accuracy.

Our final optimized model indicated that AGB can be influenced by vertical structures (two RH metrics), horizontal canopy conditions (CC) and site qualities (site productivity class). Similar to the results reported in previous studies in temperate hardwood and mixed forests (Table A1), RH metrics had particularly strong power relationship with observed AGB. The combination of RH70 and RH75 produced the best estimation of AGB in the optimized model instead of RH50, which had the strongest relationship with AGB in a single variable model. RH50 represents the height of median energy (HOME) and is sensitive to forest structure (Drake et al., 2002). The position of RH50 was generally near the bottom of main canopy crown and seemed insufficient to capture AGB differences among the predominant forest management practices in our study area. As our model included CC and site productivity, RH70 and RH75 might have better explanations about the canopy heights and vertical crown condition.

Inclusion of canopy cover, as an index horizontal canopy structure, improved the AGB estimation (Table 2). CC enhanced the model by differentiating the diverse horizontal conditions of forest canopy, which were mainly caused by forest management and natural disturbances. Our models presented nonlinear relationships between CC metrics and AGB observations (Fig. A1), indicating the deliquescent branching habitat might provide certain resistance to disturbance-driven canopy cover loss in temperate hardwood forests and curved the relationship between biomass volume and horizontal canopy coverage. In this study, CC was derived from CHM because lidar point-cloud-derived canopy closure presented low correlation with observed AGB (Fig. 3). The lidar point based canopy closure was calculated by dividing canopy points by ground points. Canopy closure was unable to represent the horizontal conditions of forest canopy due to high penetration during leaf-off conditions through tree canopies. In CHM, high penetration resulted 'holes' within individual tree canopies were filled using image processing algorithms. Therefore, CHM-based canopy coverage had better

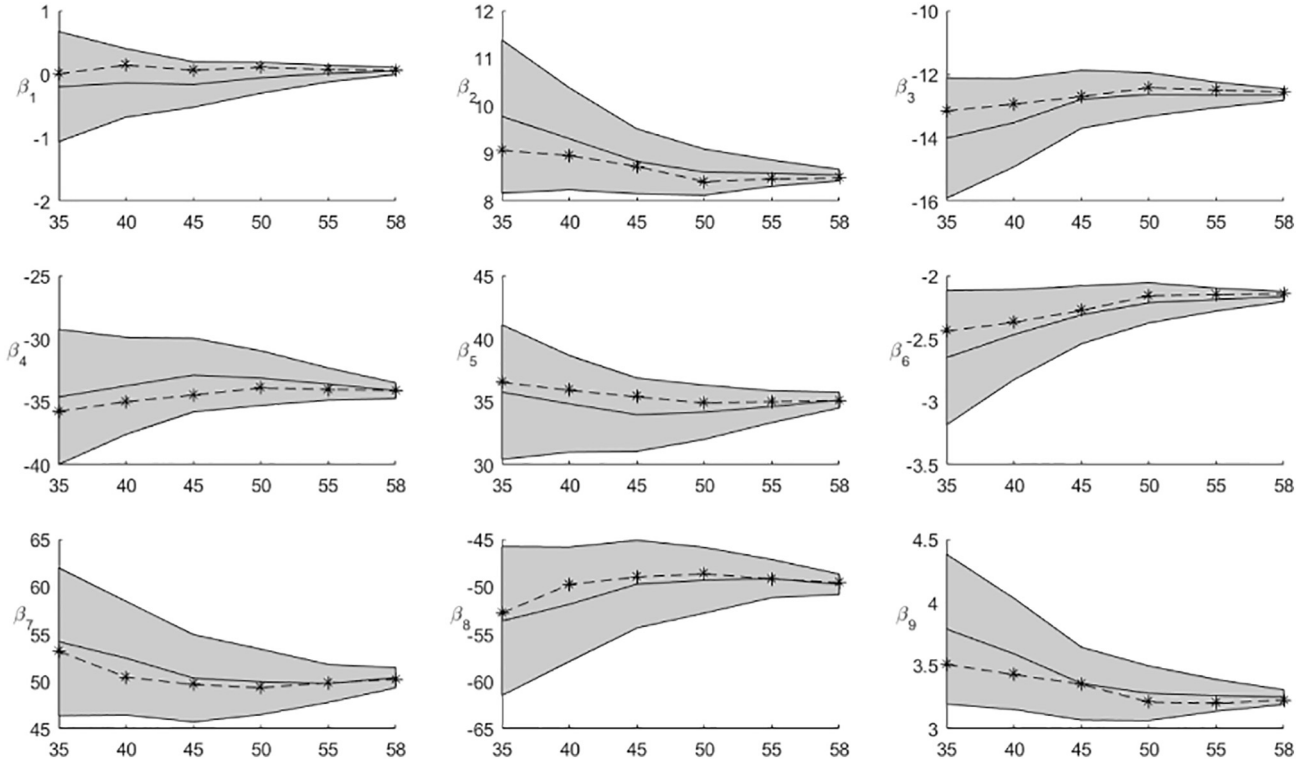

Fig. 9. Median values (dash line) and means with 96% confidence interval (gray area) of all 9 parameters in bootstrapping model validation. Horizontal axis is the number of samples used in model validation. Vertical axis is the value of simulated parameters.

explanation of horizontal canopy condition and shown stronger relationship with AGB, compared to point-cloud-based canopy closure.

Validation proved the stability of all nine parameters within our final model (Adjusted-A and B). Median values of validation statistics appeared less sensitive to outliers than mean values, particularly when using small number of samples for calculation. According to the bootstrapping analysis, there were four pairs of parameters (β_2 and β_3; β_4 and β_7; β_5 and β_8 and β_6 and β_9) (Eq. (5b)) that changed correspondingly, which means the model might only have five independent parameters. Validation also implied the reliability of the model with average R^2 value over 0.8 and that the model was robust when > 40 samples were used for calibration. The reliability and robustness make the model possible for spatial-extensive AGB estimation in temperate hardwood and mixed forests.

There are some aspects that may need to be improved in future studies. The multiplicative power regression model demonstrated its accuracy for AGB estimation in this study. However, this nonlinear function had different sensitivities to predict high and low density AGB, particularly underestimating high AGB density plots in HPS. Increasing the sample size of high AGB density plots would be possible to enhance the regression model and reduce the underestimation. Additionally, the site productivity was obtained by integrating soil map (gSSURGO) and forest inventory data, whose accuracy could be affected by the mapping unit size, raster resolution, survey methodology and classification accuracy. There are also uncertainties for soil groups without forest productivity information. Further study may be required to investigate the possibility to utilize lidar-based abiotic features (i.e. slope, elevation and aspect) to estimate the site productivity. In this study, we grouped the site productivity into binary classes (HPS and LPS) as a preliminary evaluation of its effect on lidar-based AGB estimations. Though the binary classification approach is a useful approach to understand the sensitivity of unknown variables, further improvement could be made if more sample plots across a wider range of site qualities were measured, potentially allowing treatment of site productivity as a continuous rather than a binary variable within the model.

5. Conclusion

Our optimized model had a relatively high accuracy with reliable performance in estimating AGB, integrating RH75, RH70, CC and site productivity class in a nonlinear regression model. Lidar-based RHs and CC metrics exhibited strong relationship with forest AGB, providing both vertical and horizontal variation of canopy structures. The accuracy of AGB estimations were significantly improved through weighting RHs using CC and inclusion of site productivity. Particularly, our study highlighted the impacts of site productivity on the height-oriented AGB estimation and demonstrated a framework to group soil units into productivity classes to assist lidar-based AGB estimation models in similar temperate hardwood and mixed forests.

Appendix A

Table A1
Selected lidar-based AGB studies in hardwood-dominated temperate forests.
[$] *TS = Temperate softwoods, TM = Temperate softwoods and hardwood mixed forest, TH = Temperate hardwoods forest. (Numbers in superscript match the forest type and model accuracy assessments).*
[#] *CD = Crown diameter (single-tree metric), CHP = Canopy height profile, DD = Density deciles, INT = Intensity of lidar, MaxH = Maximum of lidar height, MeanH = Mean of lidar height, RH = Relative heights, SDH = Standard deviation of lidar height.*

Reference	Location	Forest type[$]	Sensor	Plot size (ha)	Model	Predictors[#]	R^2	RMSE ($Mg\ ha^{-1}$) (%RMSE)
Anderson et al. (2006)	New Hampshire (USA)	TM[1] TH[2]	LVIS	0.07[1] 0.1[2]	Linear	RH50 (HOME)	0.61[1] 0.41[2]	58.0 (25%)[1] 46.9 (19%)[2]
Anderson et al. (2008)	New Hampshire (USA)	TH	LVIS	0.1	Linear	RH50 (HOME)	0.36	48.8 (20%)
Banskota et al. (2011)	Virginia (USA)	TH	Optech-ALTM 3100	Basal area plot	Multiple Linear	RH Kurtosis	0.64	28.5 (24%)
Duncanson et al. (2015)	California[1] Maryland[2] *N. carolina*[3] (USA)	TS[1] TH[2] TM[3]	Optech-ALTM & GLiHT	0.09	Multiple Linear	RH DD Single-tree metrics	0.85[1] 0.77[2] 0.63[3]	55.2 (15%)[1] 43.5 (40%)[2] 24.0 (12%)[3]
Hawbaker et al. (2009)	Wisconsin (USA)	TM[1] TS[2]	Leica-ALS50	0.09	Multiple Linear	MeanH SDH	0.71[1] 0.75[2]	39.3 (37%)[1] 45.6 (29%)[2]
Lefsky et al. (1999)	Maryland (USA)	TH	SLICER	0.01	Multiple Linear	CHP	0.81	61.4 (27%)
Lim and Treitz (2004)	Ontario (Canada)	TH	Optech-ALTM 1225	0.04	Power	RH	0.90	50.2 (10%)
Popescu et al. (2003)	Virginia (USA)	TH[1] TS[2]	Aero-Scan	0.02	Multiple Linear	MeanH MaxH CD	0.33[1] 0.78[2]	44.4 (34%)[1] 31.3 (39%)[2]
Sun et al. (2011)	Maine (USA)	TH	DATIS II	0.08	Multiple Linear	RH	0.71	31.3 (19%)
(van Aardt et al., 2006)	Virginia (USA)	TH[1] TS[2] TM[3]	Leica-ALS40	Basal area plot	Multiple Linear	RH INT	0.62[1] 0.63[2] 0.79[3]	39.5 (34%)[1] 12.1 (36%)[2] 16.3 (20%)[3]

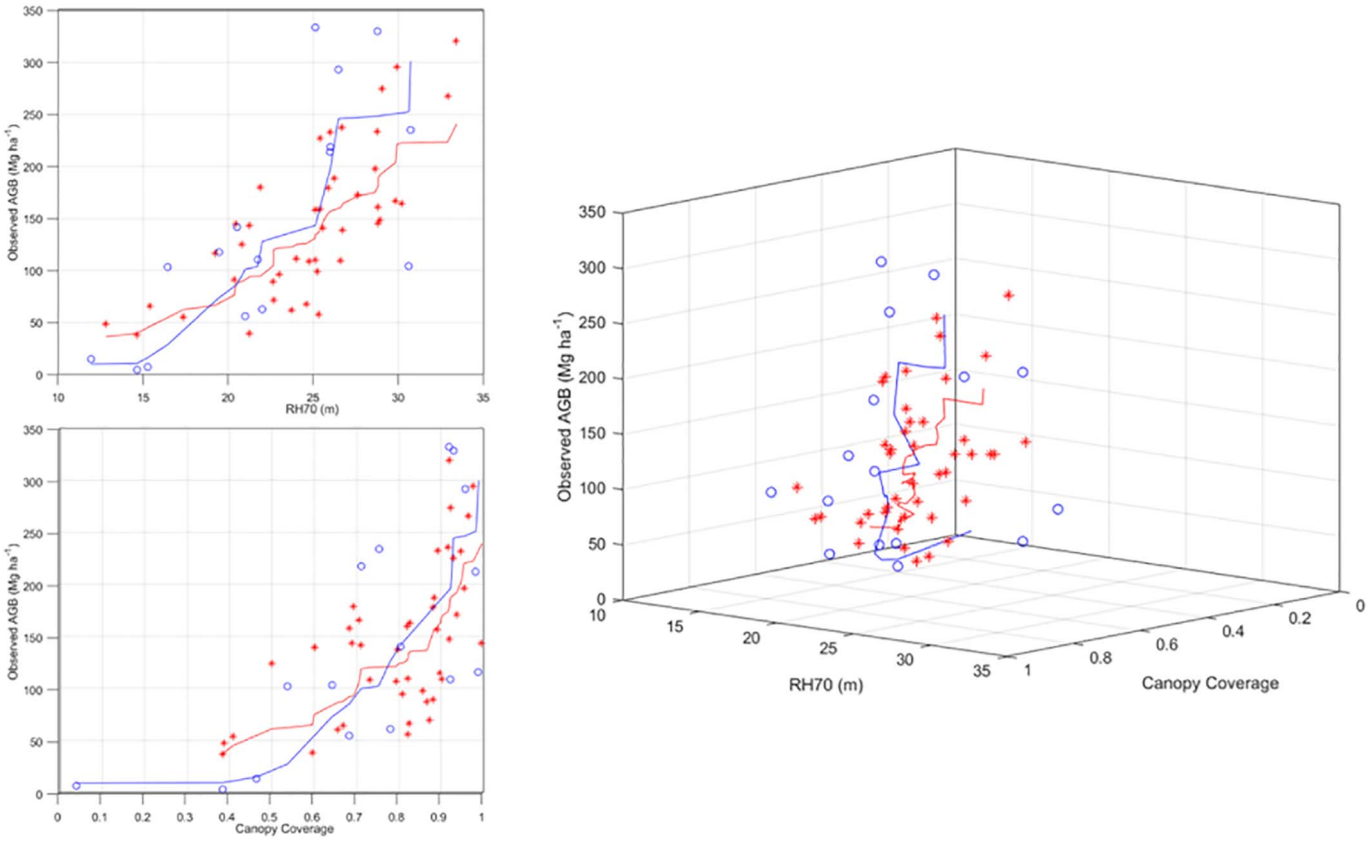

Fig. A1. Two pseudo simulation curves correlating estimated AGB with both RH70 and CC by setting the ratio between RH75 and RH70 as constant value (Eq. (5b) in Section 3.2). Red asterisks and blue cycles are HPS and LPS plots, respectively. Red and blue solid curves are the simulation curves for HPS and LPS, respectively. In the 3D graph on the right, most of LPS plots located by the left sides and the majority of HPS plots were on the right sides, indicating HPS and LPS might have different relationship between AGB and lidar-derived height and coverage. The plots in LPS had lower tree heights and larger canopy coverage compared to the plots in HPS. (For interpretation of the references to colour in this figure legend, the reader is referred to the web version of this article.)

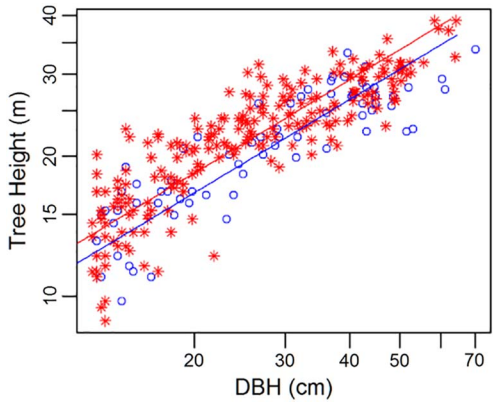

Fig. A2. Linear regression at log scale between tree height and DBH in high and low productivity sites. These two linear models were significant different in the elevations ($P < 0.0001$) and insignificant different in the slopes ($P = 0.5080$). (For interpretation of the references to colour in this figure legend, the reader is referred to the web version of this article.)

References

2011–2013 Indiana Statewide Lidar, 2016. http://opentopo.sdsc.edu/datasetMetadata?otCollectionID=OT.062012.4326.1, Accessed date: 14 November 2016.

van Aardt, J.A., Wynne, R.H., Oderwald, R.G., 2006. Forest volume and biomass estimation using small-footprint lidar-distributional parameters on a per-segment basis. For. Sci. 52, 636–649.

Anderson, J., Martin, M., Smith, M., Dubayah, R., Hofton, M., Hyde, P., Peterson, B., Blair, J., Knox, R., 2006. The use of waveform Lidar to measure northern temperate mixed conifer and deciduous forest structure in New Hampshire. Remote Sens. Environ. 105, 248–261.

Anderson, J.E., Plourde, L.C., Martin, M.E., Braswell, B.H., Smith, M.-L., Dubayah, R.O., Hofton, M.A., Blair, J.B., 2008. Integrating waveform lidar with hyperspectral imagery for inventory of a northern temperate forest. Remote Sens. Environ. 112, 1856–1870.

Asner, G.P., Powell, G.V., Mascaro, J., Knapp, D.E., Clark, J.K., Jacobson, J., Kennedy-Bowdoin, T., Balaji, A., Paez-Acosta, G., Victoria, E., 2010. High-resolution forest carbon stocks and emissions in the Amazon. Proc. Natl. Acad. Sci. 107, 16738–16742.

Banskota, A., Wynne, R.H., Johnson, P., Emessiene, B., 2011. Synergistic use of very high-frequency radar and discrete-return lidar for estimating biomass in temperate hardwood and mixed forests. Ann. For. Sci. 68, 347–356.

Basuki, T., Van Laake, P., Skidmore, A., Hussin, Y., 2009. Allometric equations for estimating the above-ground biomass in tropical lowland Dipterocarp forests. For. Ecol. Manag. 257, 1684–1694.

Boudreau, J., Nelson, R.F., Margolis, H.A., Beaudoin, A., Guindon, L., Kimes, D.S., 2008.

Regional aboveground forest biomass using airborne and spaceborne LiDAR in Québec. Remote Sens. Environ. 112, 3876–3890.
Cao, L., Coops, N.C., Innes, J.L., Sheppard, S.R., Fu, L., Ruan, H., She, G., 2016. Estimation of forest biomass dynamics in subtropical forests using multi-temporal airborne LiDAR data. Remote Sens. Environ. 178, 158–171.
Chave, J., Réjou-Méchain, M., Búrquez, A., Chidumayo, E., Colgan, M.S., Delitti, W.B., Duque, A., Eid, T., Fearnside, P.M., Goodman, R.C., 2014. Improved allometric models to estimate the aboveground biomass of tropical trees. Glob. Chang. Biol. 20, 3177–3190.
Chen, Q., Baldocchi, D., Gong, P., Kelly, M., 2006. Isolating individual trees in a savanna woodland using small footprint lidar data. Photogramm. Eng. Remote. Sens. 72, 923–932.
Drake, J.B., Dubayah, R.O., Clark, D.B., Knox, R.G., Blair, J.B., Hofton, M.A., Chazdon, R.L., Weishampel, J.F., Prince, S., 2002. Estimation of tropical forest structural characteristics using large-footprint Lidar. Remote Sens. Environ. 79, 305–319.
Duncanson, L., Cook, B., Hurtt, G., Dubayah, R., 2014. An efficient, multi-layered crown delineation algorithm for mapping individual tree structure across multiple ecosystems. Remote Sens. Environ. 154, 378–386.
Duncanson, L., Dubayah, R., Cook, B., Rosette, J., Parker, G., 2015. The importance of spatial detail: assessing the utility of individual crown information and scaling approaches for lidar-based biomass density estimation. Remote Sens. Environ. 168, 102–112.
Ferraz, A., Saatchi, S., Mallet, C., Jacquemoud, S., Gonçalves, G., Silva, C.A., Soares, P., Tomé, M., Pereira, L., 2016. Airborne Lidar estimation of aboveground forest biomass in the absence of field inventory. Remote Sens. 8, 653.
Frazer, G., Magnussen, S., Wulder, M., Niemann, K., 2011. Simulated impact of sample plot size and co-registration error on the accuracy and uncertainty of LiDAR-derived estimates of forest stand biomass. Remote Sens. Environ. 115, 636–649.
FUSION Version Check, 2016. http://forsys.cfr.washington.edu/fusion/fusionlatest.html, Accessed date: 14 November 2016.
Gallion, J., 2012. Report of continuous forest inventory (CFI)—summary of year 1–5 (2008–2012). http://www.in.gov/dnr/forestry/files/fo-CFI_Report_2008-12.pdf, Accessed date: 14 November 2016.
Hawbaker, T.J., Keuler, N.S., Lesak, A.A., Gobakken, T., Contrucci, K., Radeloff, V.C., 2009. Improved estimates of forest vegetation structure and biomass with a LiDAR-optimized sampling design. J. Geophys. Res. Biogeosci. 114.
Huang, W., Sun, G., Dubayah, R., Cook, B., Montesano, P., Ni, W., Zhang, Z., 2013. Mapping biomass change after forest disturbance: applying LiDAR footprint-derived models at key map scales. Remote Sens. Environ. 134, 319–332.
Hudak, A.T., Strand, E.K., Vierling, L.A., Byrne, J.C., Eitel, J.U., Martinuzzi, S., Falkowski, M.J., 2012. Quantifying aboveground forest carbon pools and fluxes from repeat LiDAR surveys. Remote Sens. Environ. 123, 25–40.
Jakubowski, M.K., Guo, Q., Kelly, M., 2013. Tradeoffs between lidar pulse density and forest measurement accuracy. Remote Sens. Environ. 130, 245–253.
Jenkins, J.C., Chojnacky, D.C., Heath, L.S., Birdsey, R.A., 2003. National-scale biomass estimators for United States tree species. For. Sci. 49, 12–35.
Ketterings, Q.M., Coe, R., van Noordwijk, M., Palm, C.A., 2001. Reducing uncertainty in the use of allometric biomass equations for predicting above-ground tree biomass in mixed secondary forests. For. Ecol. Manag. 146, 199–209.
Kraus, K., Pfeifer, N., 1998. Determination of terrain models in wooded areas with airborne laser scanner data. ISPRS J. Photogramm. Remote Sens. 53, 193–203.
Kronseder, K., Ballhorn, U., Böhm, V., Siegert, F., 2012. Above ground biomass estimation across forest types at different degradation levels in Central Kalimantan using LiDAR data. Int. J. Appl. Earth Obs. Geoinf. 18, 37–48.
Lefsky, M.A., Harding, D., Cohen, W., Parker, G., Shugart, H., 1999. Surface lidar remote sensing of basal area and biomass in deciduous forests of eastern Maryland, USA. Remote Sens. Environ. 67, 83–98.
Liaw, A., Wiener, M., 2002. Classification and regression by randomForest. R news 2, 18–22.
Lim, K.S., Treitz, P.M., 2004. Estimation of above ground forest biomass from airborne discrete return laser scanner data using canopy-based quantile estimators. Scand. J. For. Res. 19, 558–570.
Lim, K., Treitz, P., Wulder, M., St-Onge, B., Flood, M., 2003. LiDAR remote sensing of forest structure. Prog. Phys. Geogr. 27, 88–106.
Montesano, P.M., Nelson, R.F., Dubayah, R., Sun, G., Cook, B.D., Ranson, K., Næsset, E., Kharuk, V., 2014. The uncertainty of biomass estimates from LiDAR and SAR across a boreal forest structure gradient. Remote Sens. Environ. 154, 398–407.
Næsset, E., Gobakken, T., Solberg, S., Gregoire, T.G., Nelson, R., Ståhl, G., Weydahl, D., 2011. Model-assisted regional forest biomass estimation using LiDAR and InSAR as auxiliary data: a case study from a boreal forest area. Remote Sens. Environ. 115, 3599–3614.
NRCS Geospatial Data Gateway, 2016. https://gdg.sc.egov.usda.gov/, Accessed date: 14 November 2016.
Pflugmacher, D., Cohen, W.B., Kennedy, R.E., 2012. Using Landsat-derived disturbance history (1972–2010) to predict current forest structure. Remote Sens. Environ. 122, 146–165.
Popescu, S.C., 2007. Estimating biomass of individual pine trees using airborne Lidar. Biomass Bioenergy 31, 646–655.
Popescu, S.C., Wynne, R.H., Nelson, R.F., 2003. Measuring individual tree crown diameter with lidar and assessing its influence on estimating forest volume and biomass. Can. J. Remote. Sens. 29, 564–577.
Shao, G., Pauli, B.P., Haulton, G.S., Zollner, P.A., Shao, G., 2014. Mapping hardwood forests through a two-stage unsupervised classification by integrating Landsat thematic mapper and forest inventory data. J. Appl. Remote. Sens. 8, 083546.
Skovsgaard, J.P., Vanclay, J.K., 2008. Forest site productivity: a review of the evolution of dendrometric concepts for even-aged stands. Forestry 81, 13–31.
Skovsgaard, J.P., Vanclay, J.K., 2013. Forest site productivity: a review of spatial and temporal variability in natural site conditions. Forestry 86, 305–315.
Stark, S.C., Leitold, V., Wu, J.L., Hunter, M.O., de Castilho, C.V., Costa, F.R., McMahon, S.M., Parker, G.G., Shimabukuro, M.T., Lefsky, M.A., 2012. Amazon forest carbon dynamics predicted by profiles of canopy leaf area and light environment. Ecol. Lett. 15, 1406–1414.
Sun, G., Ranson, K.J., Guo, Z., Zhang, Z., Montesano, P., Kimes, D., 2011. Forest biomass mapping from lidar and radar synergies. Remote Sens. Environ. 115, 2906–2916.
Vepakomma, U., St-Onge, B., Kneeshaw, D., 2008. Spatially explicit characterization of boreal forest gap dynamics using multi-temporal lidar data. Remote Sens. Environ. 112, 2326–2340.
Warton, D.I., Duursma, R.A., Falster, D.S., Taskinen, S., 2012. Smatr 3–an R package for estimation and inference about allometric lines. Methods Ecol. Evol. 3, 257–259.
Wulder, M.A., White, J.C., Nelson, R.F., Næsset, E., Ørka, H.O., Coops, N.C., Hilker, T., Bater, C.W., Gobakken, T., 2012. Lidar sampling for large-area forest characterization: a review. Remote Sens. Environ. 121, 196–209.
Zhang, K., Chen, S.-C., Whitman, D., Shyu, M.-L., Yan, J., Zhang, C., 2003. A progressive morphological filter for removing nonground measurements from airborne LIDAR data. IEEE Trans. Geosci. Remote Sens. 41, 872–882.
Zhao, K., Popescu, S., Nelson, R., 2009. Lidar remote sensing of forest biomass: a scale-invariant estimation approach using airborne lasers. Remote Sens. Environ. 113, 182–196.
Zolkos, S., Goetz, S., Dubayah, R., 2013. A meta-analysis of terrestrial aboveground biomass estimation using lidar remote sensing. Remote Sens. Environ. 128, 289–298.